NATIONAL ADVISORY COMMITTEE FOR AERONAUTICS

TECHNICAL NOTE 3925

PRELIMINARY METALLOGRAPHIC STUDIES OF BALL FATIGUE UNDER ROLLING-CONTACT CONDITIONS

By H. Robert Bear and Robert H. Butler

Lewis Flight Propulsion Laboratory
Cleveland, Ohio

Washington

March 1957

NATIONAL ADVISORY COMMITTEE FOR AERONAUTICS

TECHNICAL NOTE 3925

PRELIMINARY METALLOGRAPHIC STUDIES OF BALL FATIGUE UNDER ROLLING-CONTACT CONDITIONS

By H. Robert Bear and Robert H. Butler

SUMMARY

This initial metallographic investigation included macroscopic and microscopic studies of representative samples from each lot of balls tested in the rolling-contact fatigue spin rig. SAE 52100 standard bearing steel and AISI M-1 tool steel balls were investigated at both room temperature (80° F) and at 200° to 250° F.

In this investigation fiber direction, inclusions, and chemical segregation were found to contribute much toward fatigue failures and life scatter.

Structures in the maximum-shear-stress area were stable at room temperature, but unstable when tested at 200° or 250° F. Thus, both SAE 52100 and AISI M-1 steel were sensitive to a small temperature increase.

All ball fatigue failures were visually similar and usually progressed from shear cracks. Various failure origins were found; these included chemical segregation, inclusions, surface pitting, and structure changes. Many incipient cracks were found which originated at inclusions. The ball pole regions where fiber direction is perpendicular to the surface and where inclusions and chemical segregation are more prominent were weaker areas in fatigue in the initial test runs. All failures were of the same type as those found in full-scale bearings.

INTRODUCTION

A need exists for information relative to the operation of a ball bearing above present temperature limitations in aircraft engines.

One part of such research at the NACA Lewis laboratory is the investigation of the fatigue and materials properties of the ball element of a bearing. These studies are being conducted in a rolling-contact

fatigue rig developed at the Lewis laboratory and reported in reference 1. Subsequent improvements and modifications have been made and preliminary fatigue data have been taken. The validity of the fatigue data obtained by fatigue-rig testing is reported in reference 2.

The metallographic studies presented here were made on balls which had been tested in this rig and concern the metallurgical aspects of both fatigue failure and materials behavior at room temperature and 250° F. The type of data obtainable by this method of testing is presented as well as significant physical fatigue phenomena of highly stressed balls. The opportunity to study and separate metallurgical factors is much improved compared to that provided by random ball stressing, because all the imposed stresses in this testing method are confined within a small part of the total ball surface. This work was done to evaluate and correlate spin-rig data and to obtain a basis for contemplated elevated-temperature studies. The more specific objectives were:

(1) To learn more about the causes underlying fatigue failure

(2) To study origin and progression of fatigue failures

(3) To make metallographic comparisons between the two steels under study and observe the effects of testing temperatures up to 250° F as a basis for future study of material behavior at higher temperature

(4) To compare the metallographic aspects of rig-tested balls with the available information on more standard ball-bearing testing methods

APPARATUS AND MATERIALS

Test Rig

Figure 1(a) is a cutaway view of the rolling-contact fatigue spin rig, which for brevity is often called a spin rig. The rig (described in the appendix) is based on a design reported in detail in reference 1. The test specimens are two balls revolving in a plane on the bore of the test cylinder (fig. 1(b)). Air at pressures up to 100 pounds per square inch is introduced through the nozzles to drive the balls at high orbital speeds.

The two balls separate and maintain positions 180° apart at orbital speeds to 30,000 rpm. At this speed a load of 700 pounds is obtained by centrifugal force, and a calculated Hertz stress of approximately 750,000 psi results in the center of the contact ellipse. Each ball assumes and

maintains a fixed position of rotation; this results in a track around the ball periphery. In 1 hour each ball is stressed approximately 11,000,000 times. A detailed description of the modified test rig and auxiliary equipment is given in references 2 and 3.

Test Materials and Conditions

The balls investigated were 1/2 inch in diameter and were made from SAE 52100 and AISI M-1 steels. SAE 52100 is a standard bearing steel containing 1 percent carbon and 1.45 percent chromium and is not suitable for bearing applications above 400° F (approx.). AISI M-1 steel is a molybdenum-base tool steel which maintains high hardness to approximately 800° F.

Ball geometry was modified so that the balls ran either across the poles or over the equator. Details of this modification are given in the appendix.

Metallographic examinations were made of representative balls both failed and unfailed from the groups given in the following table. Test lives varied from 1×10^6 to 200×10^7 cycles.

Material	Number of balls examined	Test temperature	Direction ball rolled (a)	Calculated Hertz stress, psi
SAE 52100	13	Room	Across poles	714,000
	20	250° F	Across poles	633,000
AISI M-1	10	Room	On equator	620,000
	30	200° F	On equator	642,000
	10	250° F	Across poles	618,000

[a]The terms poles and equators are defined in the TERMINOLOGY section.

TERMINOLOGY

Poles and equators. - Since balls are forged from cylindrical slugs which are not homogeneous but have axial flow lines, the finished ball is also not homogeneous and has flow lines. A light macroetch develops the forging flow lines; these are shown both schematically and in cross section in figure 2. These more rapidly etching pole areas are where the fiber direction is approximately perpendicular to the ball surface. The ball surface midway between the two pole areas is called the ball equator.

Ball track. - This fatigue rig concentrates all the surface contact effects on a track approximately 0.040 inch wide (fig. 3). A track area is shown in figure 3(a). Because it is a nominally rolling contact, little wear in the sense of abrasion or fretting is present. However, some discolorations, pitting, and furrowing were present and are here termed track wear conditions.

Skin effects. - Frequently, metallurgical changes occur immediately under the ball wear track. Since the depth of this condition never exceeded 0.001 inch (fig. 4), the term skin effect is considered appropriate.

Bands. - When metallurgical changes occurred under the ball track in the general area of maximum shear stress, etching revealed a band effect as in figure 4.

Incipiency. - Incipience as encountered in the discussions on inclusions and failures includes, in addition to crack initiation, some limited crack propagation. For example, the cracking around the inclusion in figure 4 shows progression yet is considered an incipient condition in relation to a fatigue failure.

METALLOGRAPHIC PROCEDURE AND TECHNIQUES

Although metallographic techniques were mostly standard, a brief summary will assist in the clarification of photographs and comments.

Sectioning. - All sectioning, especially of SAE 52100, had to be done by slow and cool grinding with a soft wheel. Cutting with a submerged water cutoff wheel resulted in severe local overheating. The majority of the balls examined were ground to the edge of the stressed track (fig. 3(a)) and parallel to it. This permitted observation of conditions under the track throughout the entire ball circumference. By regrinding at small increments, conditions under the track could be followed through its 0.040-inch width. However, some specimens were also sectioned perpendicular to the running track. Nickel plating was used on occasions to preserve pits and to minimize specimen edge bevel.

Polishing. - Specimens were polished on diamond laps to keep carbide relief to a minimum.

Etching. - Many etchants and combinations were tried to increase structure detail, which is always lacking in very fine grained martensitic steels. However, a standard 1.5-percent nital was best for structure contrast. For high magnification detail, a solution of 1 percent picral and 5 percent hydrochloric acid diluted to 1.5 percent was preferred. Five-percent electrolytic chromic acid was found advantageous for fine cracks, strains, and extremely fine carbide precipitation.

RESULTS AND DISCUSSION

Macroscopic Results

Inspection of test specimens. - All test specimens were carefully inspected at a magnification of 15 before and after testing. In an effort to reduce very early failures, many balls were given a metallographic polish to remove handling scratches and polishing burnish and to provide for even closer inspection. Polishing exposed very fine laminations in many of the AISI M-1 balls. However, tests showed that such laminations only occasionally caused early failures. Therefore, the most thorough inspection did not materially reduce ball life scatter.

Ball track conditions. - After fatigue testing, macroscopic inspection of the rolling-contact areas or ball tracks showed no correlation between running time and track conditions such as discoloration, pitting, erosion, or grooving. Apparently the variation in the condition of the ball track is from external causes, because both balls of a set showed like track conditions.

Track colorations varied from a pale straw color for the SAE 52100 balls tested at room temperature to a blue-purple on the 200° F AISI M-1 test balls. A characteristic stain pattern is shown in figure 3(a). This coloration is a very thin varnish-like layer and appears to be due to lubricant stain and oxidation within the pressure areas. Abrasive wear was absent, but metal furrowing occurred on some of the SAE 52100 specimens. Most balls showed a varying amount of pitting similar to the type often observed on gear teeth. More pitting occurred at 200° F than at room temperature. SAE 52100 specimens showed random pitting while in AISI M-1 pitting plus erosion was often shown.

Failures

The appearance of fatigue failures obtained was similar, differing primarily in the degree of spalling. They are typical of the failures encountered in service and other bearing testing methods. Figures 3(b) and (c) show failures before and after spalling. Failures were shallow, spalling to a depth of 0.004 to 0.007 inch.

Ball Macrostructures

In figure 2(b), the macrostructures of SAE 52100 and AISI M-1 show the inherent structure nonhomogeneity resulting from chemical segregation and fabrication procedures.

The ball pole regions are considered weaker regions because they receive less hot working with resultant concentration of forging fibers and nonmetallics. Initial fatigue rig runs indicated the pole areas of a ball to be weaker in fatigue. A separate investigation into the effects of fiber orientation upon fatigue life and location of failures verified a decreased life expectancy and about twice the expected number of failures in the pole regions (ref. 3). Most materials have less static strength in a transverse (to fiber) direction, and sometimes the same effect will be observed in fatigue properties (ref. 4).

A fatigue failure in the ball pole is included in figure 2(b). Since the fiber direction at the poles was parallel to the high compressive stresses, failure could originate from secondary tensile stresses. Origin and progression of fatigue failures are shown and discussed in the section Metallographic Results.

As in many macroscopic studies, more questions were raised than were answered, yet this work gave direction to the microscopic results to follow.

Metallographic Results

Inclusions and incipient failures. - This investigation showed that inclusions contribute to ball fatigue failures and life scatter. Inclusions under the ball tracks to an average depth of 0.028 inch are metallurgical stress raisers which initiate cracks. These cracks enlarge and propagate under repeated stress, becoming potential failures varying in degree as shown in figure 5.

Figure 5(a) shows representative inclusion damage about which the following observations can be made:

(1) These cracking conditions are the rule rather than the exception.

(2) The angles of cracking generally are approximately 45° to normal, that is, they are in the maximum-shear plane.

(3) When inclusions are segregated, there is a tendency toward crack alinement.

The ball of figure 5(a) had been tested for 41×10^7 cycles without failure, so these defects are not too serious. However, figure 5(b) shows the damage that a single, medium-sized (0.0015-in. diam) inclusion can do in approximately 8×10^7 cycles, even though it is located appreciably deeper than the maximum-shear-stress area.

Balls have a very hard matrix which is sensitive to loading and environmental variables. Imposed thereon during fatigue testing is a complicated and cyclic stress pattern. Therefore, close correlation of incipient cracking with running time could not be expected.

Qualitative generalizations can be made if it is noted that the location of an inclusion with respect to the maximum shear stress is of prime importance. Observations regarding inclusions common to both SAE 52100 and AISI M-1 were as follows:

(1) Inclusion hardness affected the amount of matrix cracking. The softer sulphides produced less matrix cracking than the harder oxides. Occasionally very hard angular yellow colored inclusions, probably a nitrogen-rich solid solution of titanium nitride and titanium carbide, caused the most severe cracking conditions. All of these inclusion types are shown in figure 5(c).

(2) Crack initiation begins within 1×10^7 cycles. With increased running time, more inclusions became affected, thus there was a general trend toward an increased amount and degree of cracking. Steel cleanliness is, of course, another variable.

(3) Effects of variation in inclusion size are depicted in figure 5(d). Small laminations found only in AISI M-1 steel can be serious hazards (see fig. 5(e)).

(4) In balls with short test runs (8×10^7 cycles), inclusions caused matrix cracking under the stressed track to a depth of approximately 0.023 inch; this depth increased to 0.040 inch in long tests.

There were also variations in the effect of inclusions between SAE 52100 and AISI M-1 materials. Inclusions were more numerous in SAE 52100 steel; however, the majority were of the less harmful sulphide type. Although oxides initiated severe local matrix cracking in SAE 52100, crack propagation was less than for AISI M-1 steel. No instances of crack propagation such as shown in figure 5(b) were encountered in SAE 52100 steel.

Figure 5(f) shows comparative matrix cracking produced by an oxide and by a sulphide inclusion in an SAE 52100 ball tested at room temperature. Also shown is that, although the matrix is severely cracked, crack propagation was limited, since this ball had a longer than average life of 45×10^7 cycles.

Compared to balls run at room temperature, the incidence of inclusion cracking at 200° F was much decreased in SAE 52100 steel. The sulphides seldom initiated cracking, and only the larger more critically located oxides caused matrix cracking.

In AISI M-1 steel the carbides are larger and also cause incipient failure similar to inclusions. This is shown in figures 5(g) and (h). Figure 5(g) is a segregated carbide streak in a ball pole area, and in figure 5(h) the large carbide has been split in half by the concentrated high stresses. Note also that with normal etching the incipient failure progressing from the split carbide shows no cracking and remains unetched. Likewise the damaged matrix caused by the heavy scratch to the lower right remains unetched. This indicates a similar severe straining condition and is in contrast to the brittle matrix cracking observed in SAE 52100 balls (fig. 5(f)).

Some of the incipient failure regions, as in figure 5(i), were large enough for hardness measurements and showed hardnesses approximately 3 Rockwell C points higher than the surrounding matrix. This again indicates severe straining. In order to further establish the nature of such areas, this specimen was etched with electrolytic chromic acid (fig. 5(j)). This showed that these failure areas are a combination of very fine cracks and amorphous metal.

The oxides in AISI M-1 were more numerous than in SAE 52100 and frequently were segregated to cause small laminations (fig. 5(e)). The incidence of incipient cracking around all inclusions showed a slight decrease at the 200° F testing temperature. However, crack propagation, which showed a decided decrease at 200° F for SAE 52100 balls, was appreciably increased in AISI M-1 balls.

In summation, inclusions in this study were shown to cause stress concentrations resulting in incipient failures of varying degree. Although the majority of matrix cracking observed did not terminate in a ball fatigue failure, inclusions are responsible for some failures. Figure 5(k) shows a ball failure attributed to the inclusion marked by an arrow.

Inclusion and material characteristics can be summarized as follows:

(1) Inclusion location is of primary importance. Size and orientation are also important.

(2) The oxides and larger carbides are more harmful than the softer sulphide inclusions.

(3) A decided decrease in crack formation was shown for SAE 52100 with increase of testing temperature from room temperature to 250° F.

(4) In AISI M-1 a slight decrease in matrix crack formation was observed at 250° F. However, a decided increase in crack propagation tendencies was indicated.

(5) The nature of incipient failures in AISI M-1 indicated a more ductile matrix than in SAE 52100 steel.

(6) Inclusions, carbides, and matrix conditions appeared slightly less harmful in fatigue in SAE 52100 balls than in AISI M-1 balls.

Structure Changes in SAE 52100 Balls

Testing temperature was observed to be a critical factor in producing the structure change observed in the area of maximum shear stress in SAE 52100 balls. Details of these observations follow.

Tests at 250° F. - The occurrence of a change of structure in the high-shear-stress region of a bearing race was first reported in reference 5. Such changes of structure formed a dark etching band under the stressed track of SAE 52100 balls tested at 250° F. This condition is shown in figures 6, 7, and 8. The specimens were nickel plated to preserve ball track conditions and to reduce edge bevel. Figures 6 and 8 are longitudinal views midway through the 0.040-inch-wide track after 3×10^7 and 31×10^7 cycle tests. Figure 7 is a transverse section after a 10×10^7 cycle run.

The changes of structure are the result of additional tempering to a stage called troostite. A combination of thermal and strain energy in the maximum-shear-stress regions of the ball is believed to cause this change. Comments and highlights of this condition as shown in the composite photomicrographs are itemized here to simplify reading and reference:

(1) The background photographs of figures 6, 7, and 8 are section views of a ball diameter and show the bands to be uniform in density and width. The inset views with the included micrometer scale enable band measurements to be made. They also show limited structure detail and Tukon indentations. Inset views magnified 750 times are included to show the structure detail in the troostite areas.

(2) The edges of these bands are acicular, occasionally with directional tendencies as shown in inset C of figure 6. This is believed to be an intermediate condition of tempering because it is more prominent in balls with short testing times. Inset C of figure 6 also includes an incipient failure with an entrapped area of dark etching matrix, which raises a speculative question: What was the source of the temperature rise which caused a structure change in this area?

(3) From the amount of band formed in 3×10^7 cycles (fig. 6), this structure change apparently begins soon after test initiation. With increased time, the troostitic bands become wider and more dense, as a comparison of figures 6 and 8 indicates.

(4) In the areas between the ball surface and the bands, such as area Y in inset B of figure 7, no structure change could be detected, although a slight softening compared to average matrix hardness was usually indicated. These hardness results are discussed in item (5) of the Hardness Summary. In long runs, such as the 31×10^7 cycle run of figure 8, this area between the band and the surface also becomes troostitic. This is the area labeled Y in inset D of figure 8 and the structure is identical to that of the band (area W). There is a meeting of bands at area X on this photomicrograph because of band widening and structural change under the ball track.

(5) In about 10×10^7 cycles many very fine cracks develop in the troostite areas. Insets A and D of figure 7 show such cracks; they are partially obscured by the dark matrix etching, however. In this transverse view, the cracks are parallel to the track, being more numerous in the center of the elliptical band. With longer running times, these shear cracks enlarge and elongate as in inset A of figure 8. Inset B of figure 8 is a higher magnification of these shear cracks. In this longitudinal view the shear cracks are at an angle of 45° to the ball track and presumably result from the reduced strength caused by the structure change.

(6) The hardness decrease in the troostite areas was less than expected. A Rockwell C hardness of 61 was measured, compared to an average ball hardness of Rockwell C-63 to 64 for the unchanged structure.

(7) The ball failures included in figures 6 and 7 are typical of those encountered at 250° F. They are shallow, showing a tendency not to penetrate into the troostitic band, but rather to skim along its edge. This tendency may be caused by collapse of the harder layer resulting from insufficient support from the softer underlying troostite band. Ball failures are discussed again in the section Origin and Progression of Ball Failures.

Tests at room temperature (80° F). - Aside from the inclusion damage already discussed, the balls at room temperature showed no structural change. Figures 9(a) and (b) are comparison photomicrographs of one untested ball with another that ran for 200×10^7 cycles without a failure.

The room-temperature runs were at a stress of 714,000 psi and those at 250° F at a stress of 633,000 psi. Other test conditions such as lubrication were unchanged. Therefore, testing temperature appears to be a critical factor effecting the structure change already discussed for SAE 52100 steel.

Structure Changes in AISI M-1 Balls

Contrary to expectations, structures in AISI M-1 balls were unstable in the maximum-shear-stress region. This instability was slight at room temperature but prominent in balls tested at 200° F. These initial studies indicate a work hardening effect rather than a change in structure.

Tests at room temperature (80° F). - The as-received AISI M-1 ball structures were as shown in figure 9(c). Figure 9(d) is a representative subtrack structure after 44×10^7 cycles. There were slight structure changes in some of the balls tested at room temperature such as:

(a) The prior austenite grain boundaries became less pronounced.

(b) There was a narrow light etching skin effect at the track.

(c) Occasionally a fine feathering constituent resembling a secondary hardening effect was observed.

These results were not prominent at room temperature, but at 200° F were prominent enough to be better evaluated.

Tests at 200° F. - Since AISI M-1 steel is double-tempered at 1050° F, no structure changes were expected. When banding conditions similar in some aspects to those in SAE 52100 were encountered, additional studies were made.

Such subtrack changes are shown in figure 10(a). The changed structure etches as a light rather than a dark band. Although etching characteristics are reversed, the bands are similar to SAE 52100 in size and area of origin and become more prominent with increased running time. Bands expand out to the surface as in the long running ball (111×10^7 cycles) in figure 10(b). However, they do not progress into the ball beyond a depth of 0.011 to 0.013 inch. The two white jagged lines approaching the ball surface (fig. 10(b)) are fatigue failure progressions originating from a small lamination beyond this photomicrograph.

AISI M-1 balls also showed banding characteristics different from SAE 52100. They originated and progressed more slowly with increased cycling and developed no shear cracks. Band occurrence and progression were more erratic than in SAE 52100.

The time-life relation of the structure change is shown in figure 11. These are transverse views of representative 4×10^7, 20×10^7, and 111×10^7 cycle runs and include high-magnification views of the microstructures from the band centers. In short-run balls, structure changes

resembled possible secondary hardening effects. However, as these changes developed with increased time, a work hardening or straining of the matrix was indicated due to overstressing in the high-shear-stress region.

Skin effects, which were observed only on the longer running SAE 52100 balls tested at 250° F, occurred more frequently in AISI M-1 steel. This structure change was less than 0.001 inch deep, and its occurrence was erratic. Figure 12(a) is an above average case of such skin effects for AISI M-1 balls. The exact nature of this condition has not yet been determined. When pitting and wear occurred on the track, cracking developed as shown. Figure 12(b) shows similar cracking in an SAE 52100 ball.

In AISI M-1 steel, therefore, structures were unstable under these high stresses at 200° F and occasionally showed very slight instability in room-temperature runs. If the slight testing temperature difference observed here is a criterion, higher bearing temperatures may present many additional problems. The material selection problem by itself could prove difficult if the instability observed here is accelerated with increasing temperature, and if other high-temperature steels show a similar instability to high stresses.

Origin and Progression of Ball Failures

The sensitive shutoff mechanism in the spin rigs provided many small incomplete failures for examination. Failures are not due to a single mechanism even though there is a similarity in appearance and progression (spalling), as noted in the macroscopic investigation.

Very early failures (in less than 5×10^6 cycles) are believed due to defective material not discernible by stringent preinspection. Several groups of balls were sectioned and examined in the as-received condition. Occasional defects, generally in the pole areas, were found such as shown in figure 13.

Inclusions and their failure potentialities were previously discussed, yet very few completed failures were encountered which could be definitely attributed to inclusions. Either they do not cause most failures, or the proof of damage is destroyed during the failure process. It was shown that inclusions are cracked and often crushed during endurance testing, so that their retention even in an incompleted failure such as shown in figure 14(a) is improbable. A large inclusion is only 0.001 inch in diameter, which is less than the width of the major cracks in a failure.

Figure 14(a) is an SAE 52100, room-temperature, pole-area failure showing failure origin and progression. Chemical segregation is parallel

to the high compressive stresses. Such structure inhomogeneity can result in changes in elastic modulus, or act as a metallurgical stress raiser. It is believed that secondary tensile stresses normal to the chemical segregation were too high, causing the fatigue crack indicated by arrow A in figure 14(a). Arrows B show shear cracks progressing from the original fatigue crack. A completed failure of such origin is shown in figure 14(b). A slight variation, whereby failures initiate and progress in shear cracks, is shown in figure 15(a), which shows the first spalling and the progressive spalling that follows.

Ball spalling averaged 0.005 inch in depth. Room-temperature SAE 52100 failures exhibited the deepest flake-outs and a more brittle type of cracking.

Typical SAE 52100 failures at 250° F were included in the photographs of figures 6 and 7. The partial failure in inset A of figure 6 appears to be representative of failure origin and initial propagation. No evidence that the structure change in the band took a direct part in these shallow failures was found in this investigation. However, these bands probably contributed indirectly to the failure by loss in strength, internal stresses resulting from volume changes and the less ductile matrix layer between the ball surface and the troostite band.

In AISI M-1 balls the fatigue failure mechanism was also shear. Figure 15(b) illustrates a failure at room temperature, and figures 15(c) and (d) are representative failures at 200° F. Again fractures appear to be slightly more brittle at room temperature. Cracks are widest below the ball surface and penetrate into the band area. These views are sections through the ball equator and therefore show no fibrous structure.

When surface pitting or skin effects are prominent, fine subsurface cracks often occur, as shown in figure 16(a); figure 16(b) shows the same area etched. Initial small spalling can develop into a large failure; figures 16(c) and (d) show such a failure progression.

Failures originate within 0.005 inch of the ball surface and result primarily from shear cracking, although some failures indicated origin from secondary tensile stresses. Adverse surface conditions such as pitting or skin effects can also initiate a fatigue failure. The initial failure is a very small spall such as pictured in figure 15(a), which also shows the failure progression.

Hardness Summary

Many Tukon hardness surveys were made. A few of these are included with the photomicrographs used in the preceding discussions. Rockwell C

equivalents are given in place of the Knoop hardness numbers. These hardness studies were less decisive than expected, many hardness trends falling within the error margin of testing. Carbides prevented obtaining true matrix hardness values. A summary of hardness testing is as follows:

(1) No decisive hardness differences were indicated between SAE 52100 and AISI M-1 balls, or between the as-received and the endurance-tested balls.

(2) The troostitic bands in SAE 52100 showed a slight hardness decrease but not as great a decrease as the change in structure indicated.

(3) In the banded areas in the AISI M-1 balls hardness values were indecisive, although slight hardness increase trends were indicated in some of the more severly banded balls.

(4) The skin effects in AISI M-1 steel, in the few places that were deep enough to be tested, showed softening.

(5) It can be observed on the photomicrographs that the first hardness value next to the ball surface indicates softening. This same effect was found on as-received balls and is apparently an edge effect, since these balls when tested at light loads showed no softening. However, in long-run balls, light load hardness values indicated that slight softening took place. More effort is required in this field.

SUMMARY OF RESULTS

This metallographic investigation was made on representative 1/2-inch balls after fatigue testing in the rolling-contact fatigue spin rig. Test runs were made at room temperature and either 200° or 250° F on groups of balls of SAE 52100 and AISI M-1 steels. All balls contained 0.050-inch-diameter drilled holes which predetermined the direction of testing, which was either across the ball poles or on the ball equator. The following results were obtained:

1. Structures in the maximum-shear-stress area were stable at room temperature but unstable when tested at 200° F. Thus, both SAE 52100 and AISI M-1 steel were sensitive to a small temperature increase. In SAE 52100 this structure change was a tempering of the original matrix to a stage called troostite. In M-1 steel, matrix work hardening or strain is indicated. In the direction parallel to the stressed track, these areas appeared as a band increasing in width and intensity with running time. Bands extended to within 0.002 or 0.003 inch of the ball

surface except in long-run tests when they progressed to the ball surface. Shear cracks which occurred in the bands of SAE 52100 balls after sufficient testing time were not encountered within the bands of AISI M-1 balls.

2. Inclusions were found to be a definite hazard to fatigue life. They are stress raisers causing local matrix cracking. Although inclusions were not found in many of the failures, this is probably because of the fact that the average inclusion is minute compared to the size of the average spall. Many incipient cracks were found which originated at inclusions. These cracks propagated in varying amounts depending on inclusion size, location, and type and the condition of the surrounding matrix. In SAE 52100 both cracking incidence and propagation were decidely less at 250° F than at room temperature. AISI M-1 showed only a slight decrease in cracking incidence at 200° F over that at room temperature but with a definite tendency for cracks to enlarge and propagate at 200° F. In addition, the larger carbides in AISI M-1 caused frequent matrix cracking. Although the majority of these incipient failures did not assume serious proportions even after many stress cycles, some of the large fatigue scatter and early failures are attributed to inclusions. It is difficult to correctly evaluate inclusions as a failure cause, because they are usually destroyed in the failure process.

3. The ball pole areas, where the forging flow lines are approximately perpendicular to the ball surface, are metallurgically inferior regions because of less hot reduction in these areas and the resulting concentration of chemical segregation and nonmetallics.

4. All failures were of the same type as those found in full-scale bearings.

5. Even though the SAE 52100 and AISI M-1 failures were similar in appearance, various causes for failure were indicated. They are:

a. Chemical segregation and fiber direction

b. Change of structure in the maximum-shear-stress area

c. Inclusions

d. Track conditions such as skin effects, pitting, and surface laminations

Except for failures resulting from track conditions, subsurface failure origin is indicated. Most failures originated only 0.002 to 0.006 inch below the track surface. In most ball failures the failure mechanism was shear.

6. Occasionally very shallow structure changes (max. depth, 0.001 in.) occurred immediately under the stressed surface. These skin effects were encountered on SAE 52100 balls only after long runs at 200° F. The skin effects occurred more frequently in AISI M-1 balls in both room-temperature and 200° F endurance runs. Their cause or nature was not definitely established. This condition can initiate shallow surface spalling and result in ball failure.

7. Tukon hardness surveys were less decisive than expected, many hardness trends falling within the error margin of testing. Small matrix hardness variations appeared to be obscured by the presence of carbides. The troostite band areas showed slight softening, and the bands in AISI M-1 balls occasionally showed a slight but indecisive hardness increase. Further study is required in this field.

8. It can be assumed that local factors and variables are inherent in ball bearings that were either overlooked or not encountered in this initial study. Since fatigue failures are sensitive to very small local factors, the ball life dispersion, which was difficult to accept before these studies, now appears more acceptable. If the metallographic results observed here are a criterion, a high-temperature ball bearing will present many additional problems which will require a concerted research effort.

Lewis Flight Propulsion Laboratory
National Advisory Committee for Aeronautics
Cleveland, Ohio, November 27, 1956

APPENDIX - APPARATUS AND PROCEDURE

Test Rig

As is previously stated, figure 1(a) is a cutaway view of the rolling-contact fatigue spin rig. The test specimens are two test balls revolving in a plane on the bore of the test cylinder (fig. 1(b)). Air at pressures up to 100 pounds per square inch is introduced through the nozzles to drive the balls at high orbital speeds. The nozzle system and the cylinder are held together by upper and lower cover plates fastened by three removable bolts. An exhaust can to direct used air downward is fastened to the upper cover plate. In order to keep the first dynamic critical frequency of the rig as low as possible (about 150 rpm), the rig assembly is supported from a rigid frame by three flexible cables. To keep external constraint at a low value, the drive air is introduced into the rig through a 6-foot-long flexible metal hose.

Rig operation. - The two test balls separate and maintain relative positions 180° apart at orbital speeds above the critical frequency. A detailed analysis of the rig operation may be had from reference 1.

Loading. - The only loading on the balls is that produced by centrifugal force and is in excess of 700 pounds for a 1/2-inch ball revolving in a 3.25-inch-bore test cyclinder at an orbital speed of 30,000 rpm. This will develop a maximum Hertz stress of approximately 750,000 pounds per square inch in the center of contact.

Lubrication. - Lubrication is accomplished by introducing droplets of the lubricant into the drive airstream between the guide plates (fig. 1(a)). The rotating airstream forces the droplets against the bore of the test cylinder.

Lubricant flow rate is controlled by controlling the pressure upstream of a long capillary tube. The pressure drop through the capillary was sufficient to give excellent control of the flow for small flow rates. The lubricant flow rate used in both series of tests was approximately 5 milliliters per hour. The lubricant used in these ball tests was a synthetic diester which met the MIL-L-7808 specifications for aircraft turbine engine lubricants except for the low-temperature viscosity requirement.

Instrumentation. - The two major instrumentation systems of the rig are a speed measurement and control system and a failure detection and shutdown system.

Orbital speed is measured by counting the pulses from a photoamplifier on an electronic tachometer. The pulses are generated by the two test balls interrupting a light beam to the photocell.

Failures are detected by comparing the amplified signal from a velocity-type vibration pickup (attached to the rig, see fig. 1(a)) with a predetermined signal level that is preset on a meter relay. The large vibration amplitude resulting from a ball or cylinder failure trips the meter relay which shuts down the test.

The only other instruments used were pyrometers for measuring and controlling temperatures of the drive air and the test rig.

Air supply. - The drive air is dried to less than 30 percent relative humidity and then filtered before being used in the rigs. When temperature tests were run, the air was preheated in an electric furnace.

Materials

The ball and cylinder materials chosen to be tested were SAE 52100 and AISI M-1. SAE 52100 is the standard steel used for precision ball and roller bearings and was chosen for reference purposes. AISI M-1 was chosen because some experience had been obtained with this steel in laboratory tests and field applications.

Test Specimens

Cylinders. - The dimensions of the test cylinders are as follows: outside diameter, 4.750 inches; length, 3.00 inches; initial nominal inside diameter, 3.250 inches. The bore surface finish was 2 to 3 microinches for all cylinders. Roundness of the bore was held to 0.0001 inch and bore taper to a maximum of 0.0003 inch. Hardness measurements were taken on the cylinder ends. Each cylinder was uniform within 2 hardness numbers, although average hardness for different cylinders varied between Rockwell C-60 and 64.

Between 10 and 15 tests may be run on a bore surface. An unused bore surface is provided for each test by a vertical adjustment of the nozzle assembly (fig. 1(a)). The bore is then reground 0.060 inch larger and refinished. This new surface is about 0.022 inch below the location of the maximum shear stress of the previous tests, and so the effects of prior stressing are considered to be negligible. Failure positions on one cylinder surface do not correlate with failure positions of the previous test surface.

Test balls. - The test balls of both materials were hardened to Rockwell C-63 to 64. During manufacture the nominally 0.500-inch-diameter balls had their geometry modified by a 0.050-inch hole drilled diametrically through them. The hole was drilled parallel to or perpendicular to the forging direction. It established a fixed axis of

rotation and caused the ball to roll either coincident with the equator or over the poles. Figure 2(a) is a schematic illustration of this modification. Figure 2(b) is a macrophotograph of etched SAE 52100 and AISI M-1 balls showing the chemical segregation that is referred to as fiber orientation.

Testing Procedure

Pretest inspection. - Cylinders were given dimensional, surface finish, and hardness inspections. This was followed by a magnetic particle inspection for both cracks and large subsurface inclusions and a visual inspection for deep scratches and other mechanical damage.

All test balls were weighed and inspected at a magnification of 60. The presence of excessive scratches, pitting, any cracks, laminations, and flat spots was noted in a permanent record. Some of the balls were given a 30-minute polish on a Gamal polising cloth using levigated alumina. This resulted in a carbide relief on the AISI M-1 balls but only removed the finer scratches on the SAE 52100 balls. This procedure exposed defects (such as fine laminations and cracks) that were previously hidden by the surface finish.

Prior to inspection and use, test specimens were flushed and scrubbed with 100 percent ethyl alcohol on clean cheesecloth. This procedure left a thin film of grease on the surface, but this was considered desirable to minimize corrosion.

Assembly of rig. - The rig and test specimens were cleaned and assembled with care to prevent scratching of the bore surface. The bore surface and test balls were coated with lubricant. The test position in the cylinder was set by loosening the collet (fig. 1(a)) and moving the nozzle assembly and the test balls axially to the test station and then retightening the collet. The rig was mounted in the support frame and then leveled. Oil and air supply lines and the vibration pickup were connected. The final step was to check the alinement of the light beam on the photocell.

Starting and Running Procedure

The rig was brought up to operating speed as rapidly and as smoothly as possible. The rig could then be switched to automatic speed control or left on manual control. On manual control the rig speed must be corrected at intervals to compensate for the speed increase due to run-in of the test specimens. Run-in is rapid for the first few hours, and it is practically complete after the first 48 hours.

Speed and oil flow were monitored regularly. Speed, air pressure, and vibration levels were recorded at each reading. The test was continued until a predetermined number of stress cycles had been exceeded or until a ball or race failure actuated the meter relay which shut the rig down.

Stress calculations. - With the ball weight, speed, and orbital radius of rotation of the test balls known, the load was calculated from the relation: Force equals mass times acceleration. The stress developed in the contact area was calculated from the load and specimen geometry by using the modified Hertz formulas given in reference 5.

Post-test inspection. - After the tests the failed balls were examined at a magnification of 60 in order to determine whether surface factors were responsible for the failures.

REFERENCES

1. Macks, E. F.: The Fatigue Spin Rig - A New Apparatus for Rapidly Evaluating Materials and Lubricants for Rolling Contact Bearings. Lubrication Eng., vol. 9, no. 5, Oct. 1953, pp. 254-258.

2. Butler, Robert H., and Carter, Thomas L.: Stress-Life Relationship of the Rolling-Contact Fatigue Spin Rig. NACA TN 3930, 1957.

3. Butler, Robert H., Bear, H. Robert, and Carter, Thomas L.: Effect of Fiber Orientation on Ball Failures Under Rolling Contact Conditions. NACA TN 3933, 1957.

4. Grover, H. J., Gordon, S. A., and Jackson, L. R.: Fatigue of Metals and Structures. NAVAER 00-25-534, Dept. Navy, Bur. Aero., 1954.

5. Jones, A. B.: Metallographic Observations of Ball Bearing Fatigue Phenomena. Symposium on Testing of Bearings, A.S.T.M., 1947, pp. 35-48; discussion, pp. 49-52.

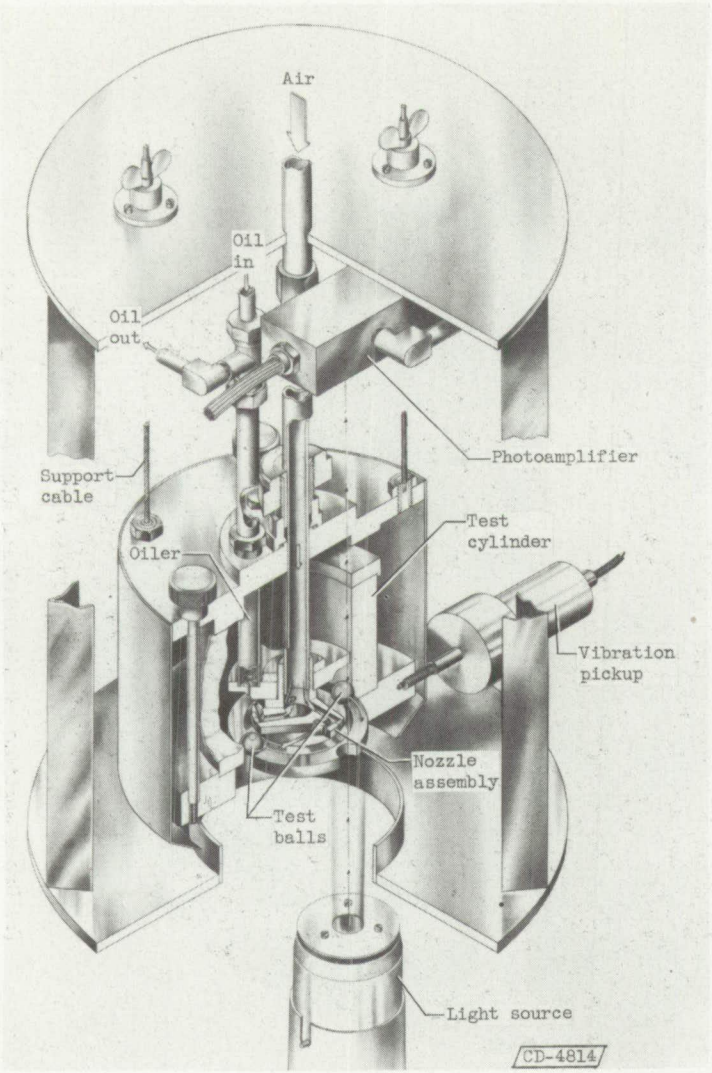

(a) Cutaway view.

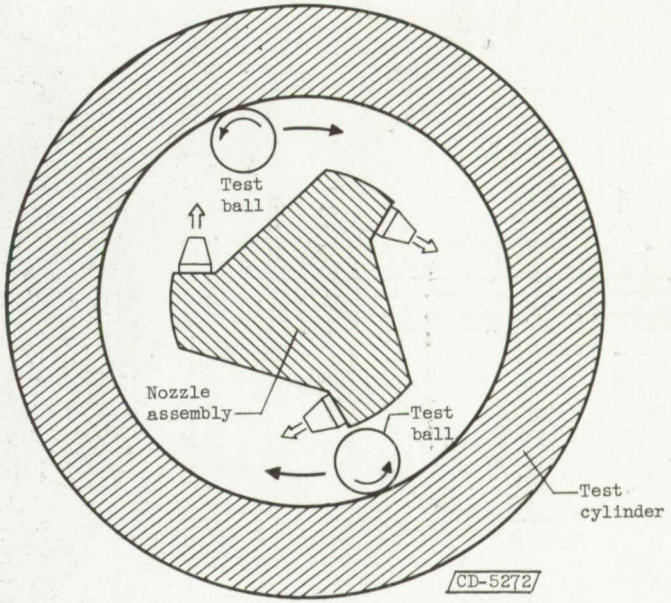

(b) Schematic diagram

Figure 1. - Rolling-contact fatigue spin rig.

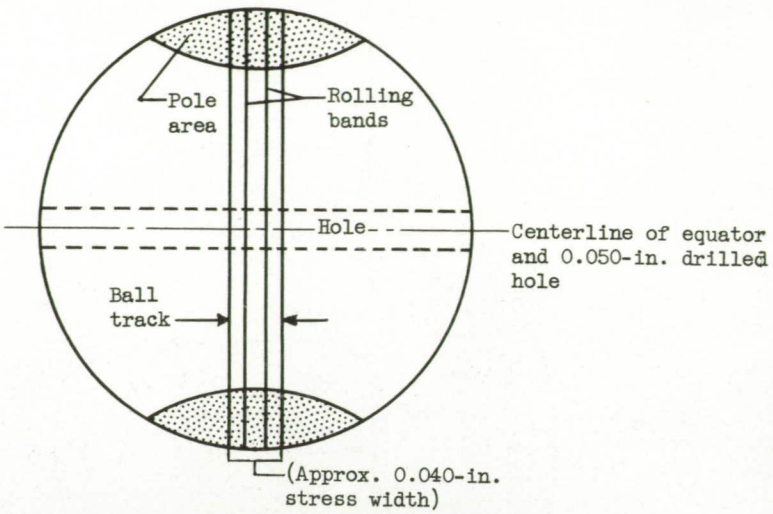

(a) Schematic drawing showing poles, test track, and ball modification (0.050-in. drilled hole).

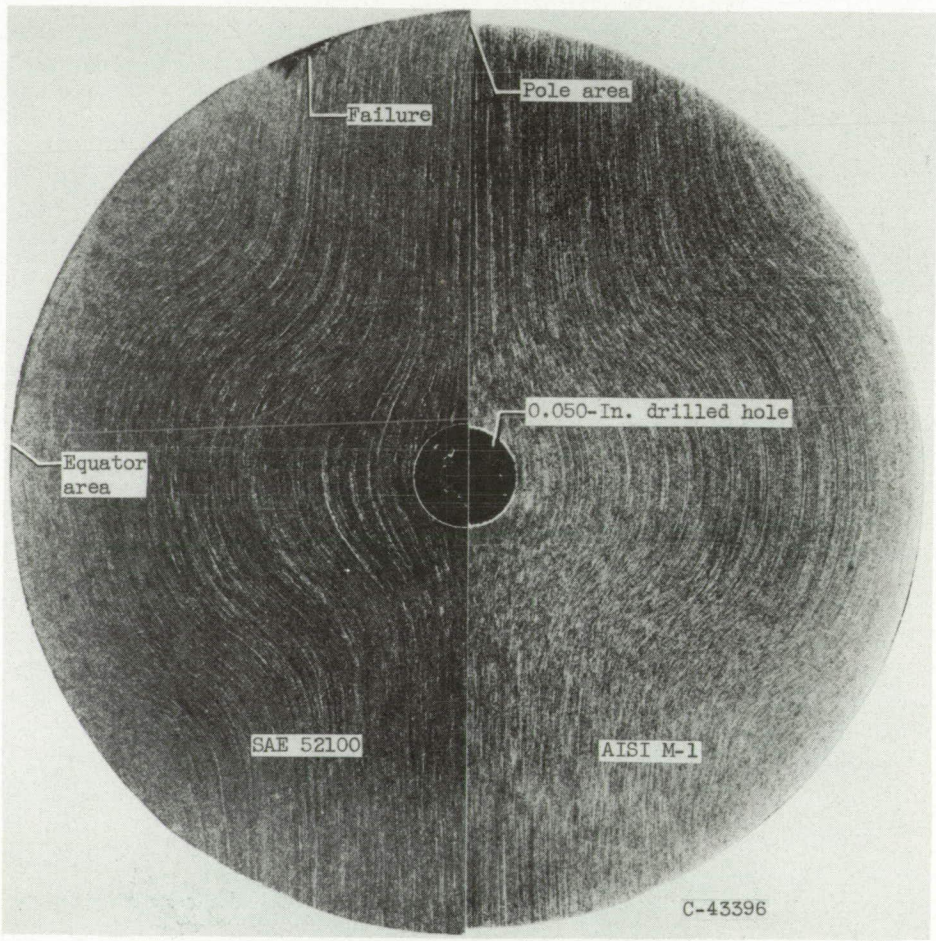

(b) Cross sections of SAE 52100 and AISI M-1 balls. X12.

Figure 2. - Ball nomenclature and structure. Figure has been decreased 25 percent in printing.

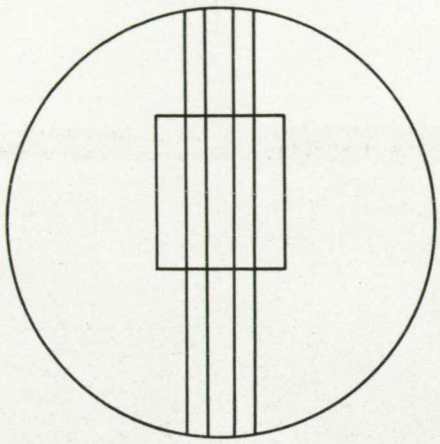

Sketch of ball showing location of areas pictured below

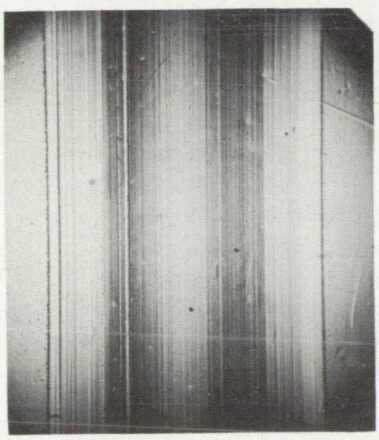

(a) Ball track.

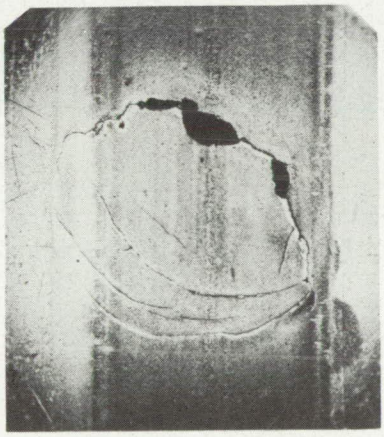

(b) Ball track fatigue failure, before spalling.

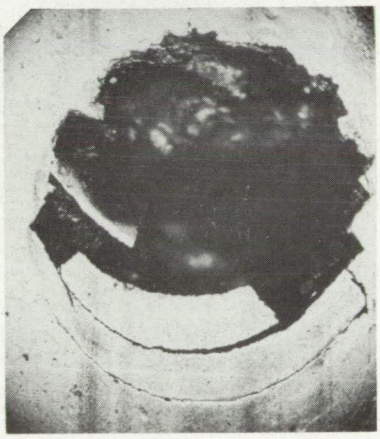

C-43397

(c) Ball track fatigue failure, after spalling.

Figure 3. - Macrosopic views of ball tracks and fatigue failures.

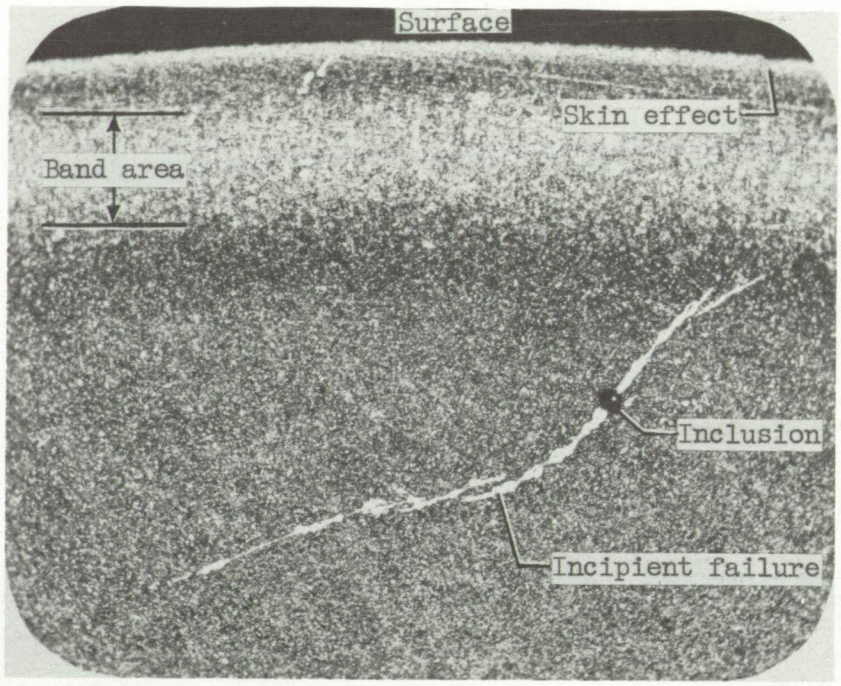

C-43398

Figure 4. - Nomenclature for defects in balls after test. X75. Figure has been printed at original magnification.

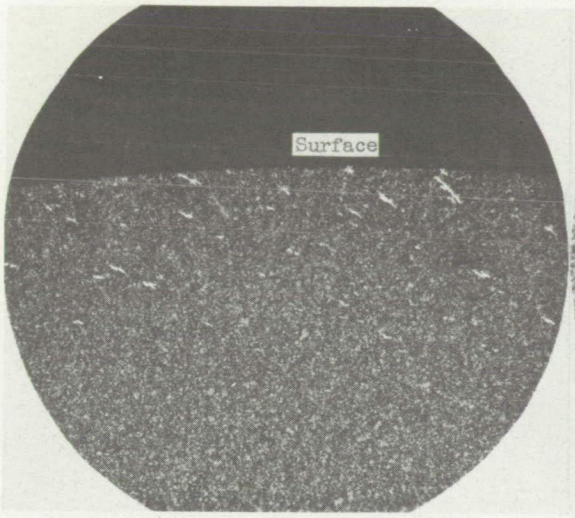

(a) Small matrix cracks caused by inclusions in AISI M-1. X75.

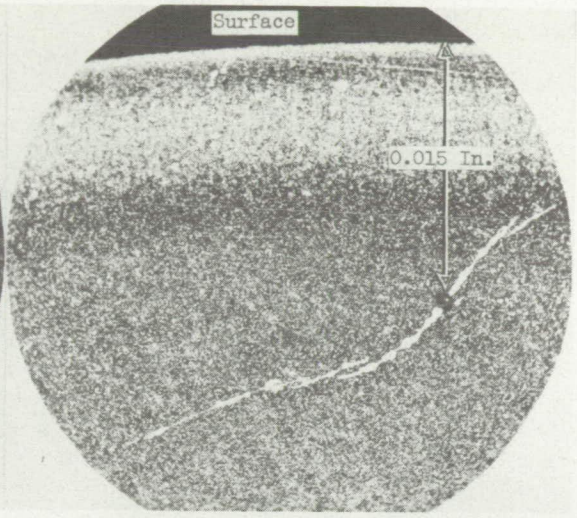

(b) Crack propagation from large inclusion in AISI M-1. X75.

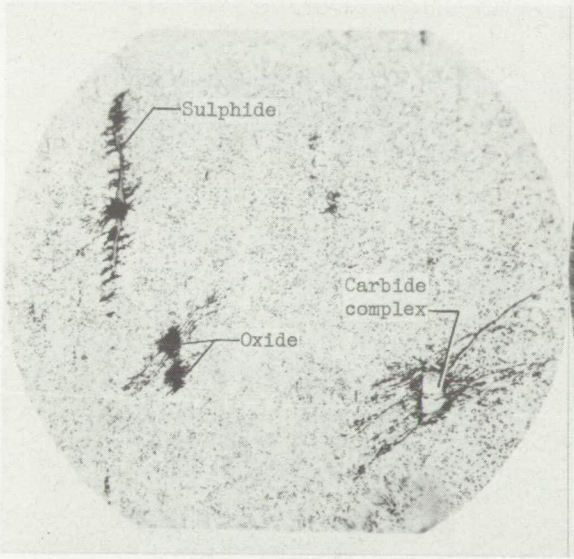

(c) Relative matrix cracking incurred by carbide, oxide, and sulphide inclusions in SAE 52100. X500.

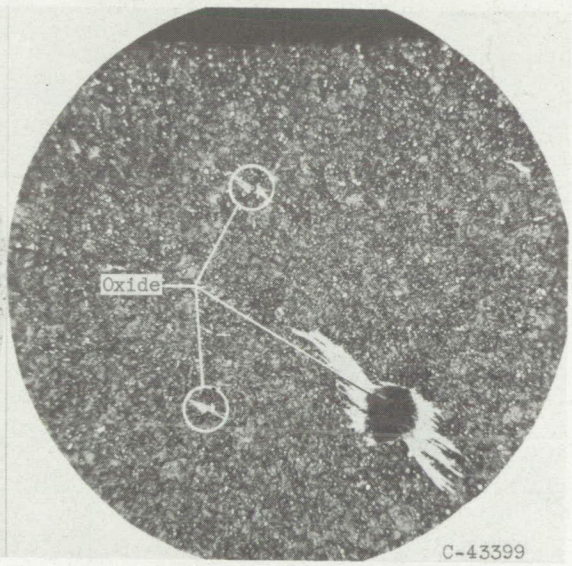

(d) Inclusion size effects and cracking in AISI M-1. X250.

Figure 5. - Inclusions and incipient failures. Figure has been decreased 25 percent in printing.

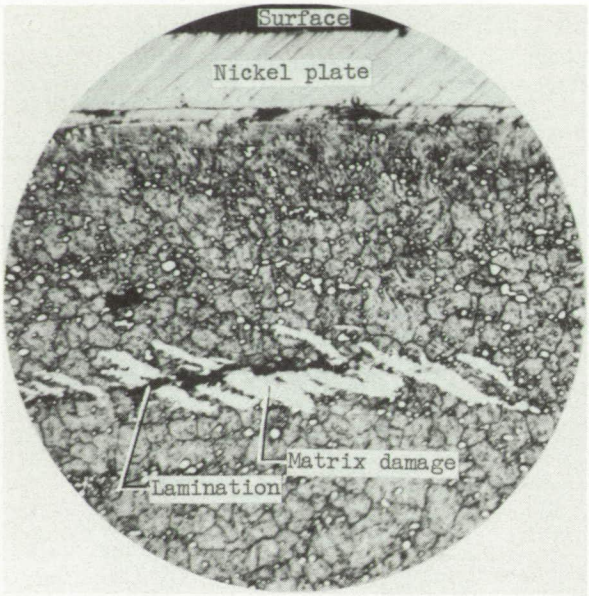

(e) Matrix damage (white) caused by lamination (black) in AISI M-1. X500.

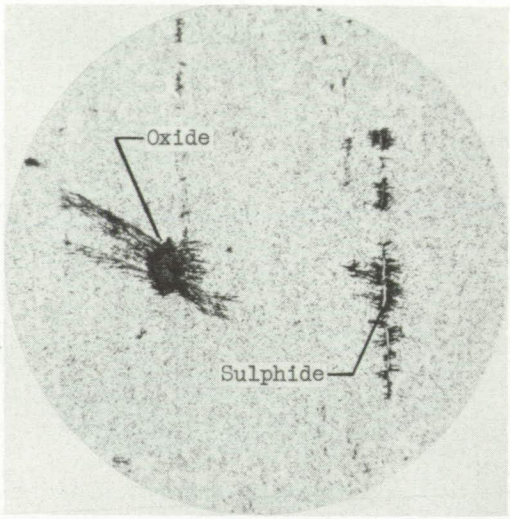

(f) Brittle type of matrix cracking in SAE 52100. X250.

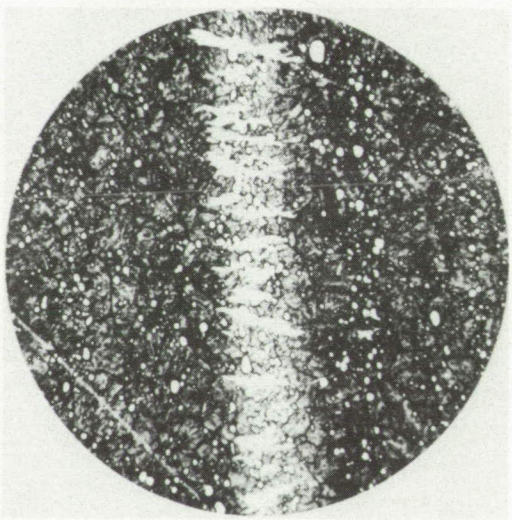

(g) Segregated carbide streak and matrix damage in AISI M-1. X500.

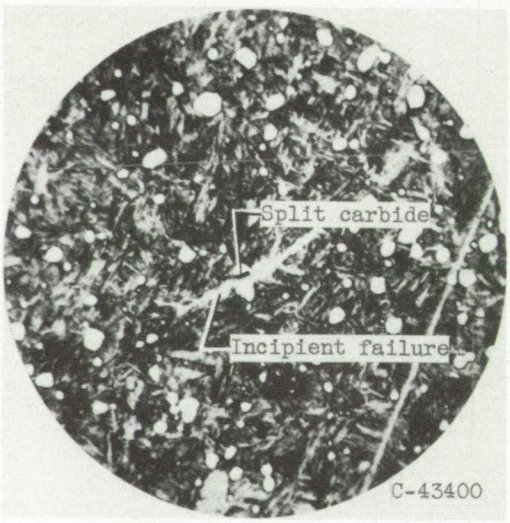

(h) Incipient failure progressing from a carbide (split) inclusion in AISI M-1. X1500.

Figure 5. - Continued. Inclusions and incipient failures. Figure has been decreased 20 percent in printing.

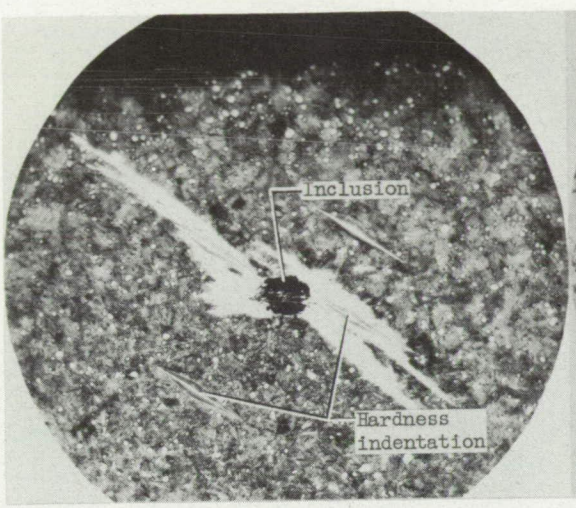

(i) AISI M-1 damaged matrix (white) showing no cracking with picral-HCL etch. X500.

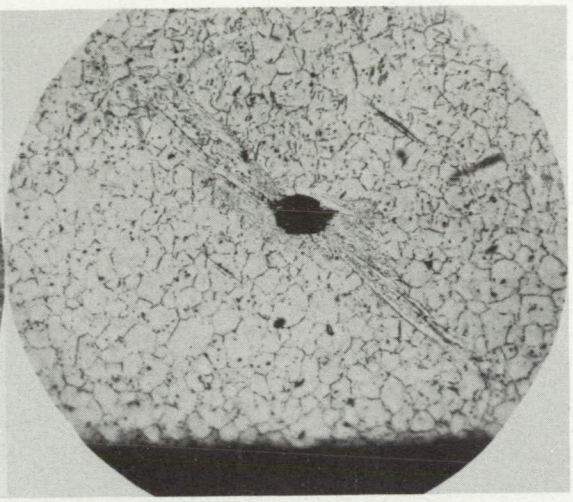

(j) Same as (i) after additional etching with chromic acid (electrolytically); shows small cracks and amorphous structure.

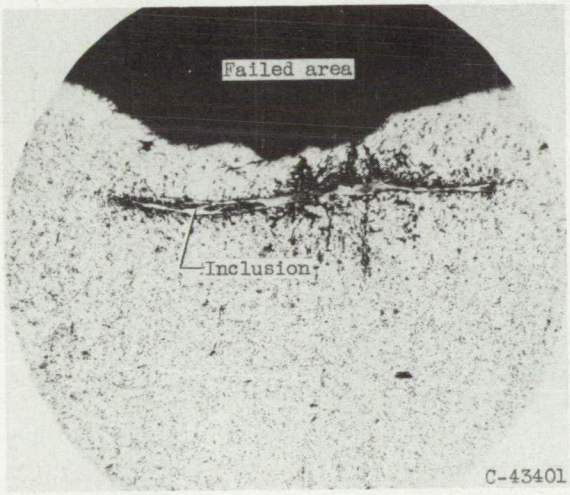

(k) Fatigue failure caused by inclusions in SAE 52100. X250.

Figure 5. - Concluded. Inclusions and incipient failures. Figure has been decreased 25 percent in printing.

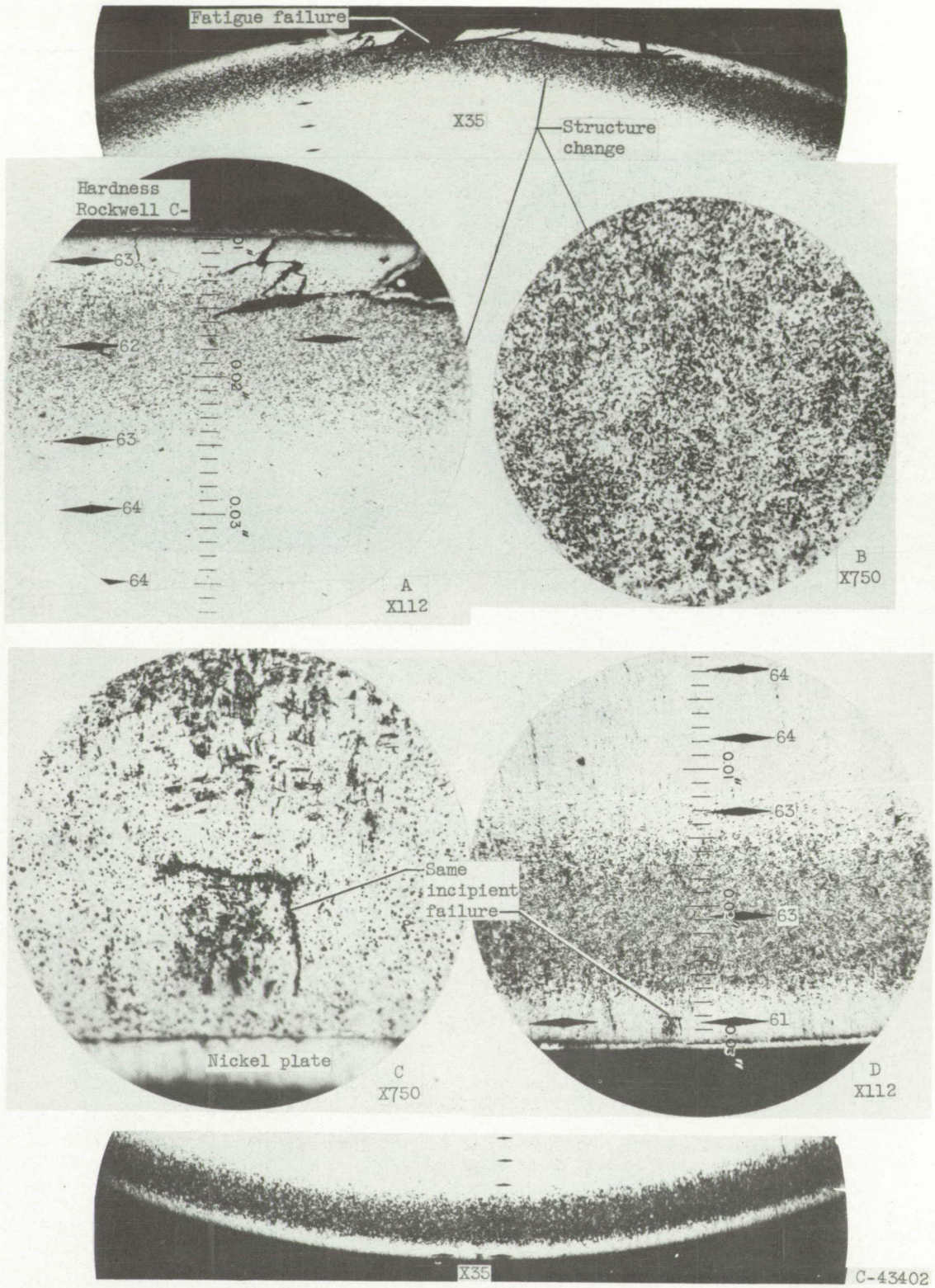

Figure 6. - Structure change in SAE 52100 tested 3×10^7 cycles at 250° F. Longitudinal view. Figure has been decreased 20 percent in printing.

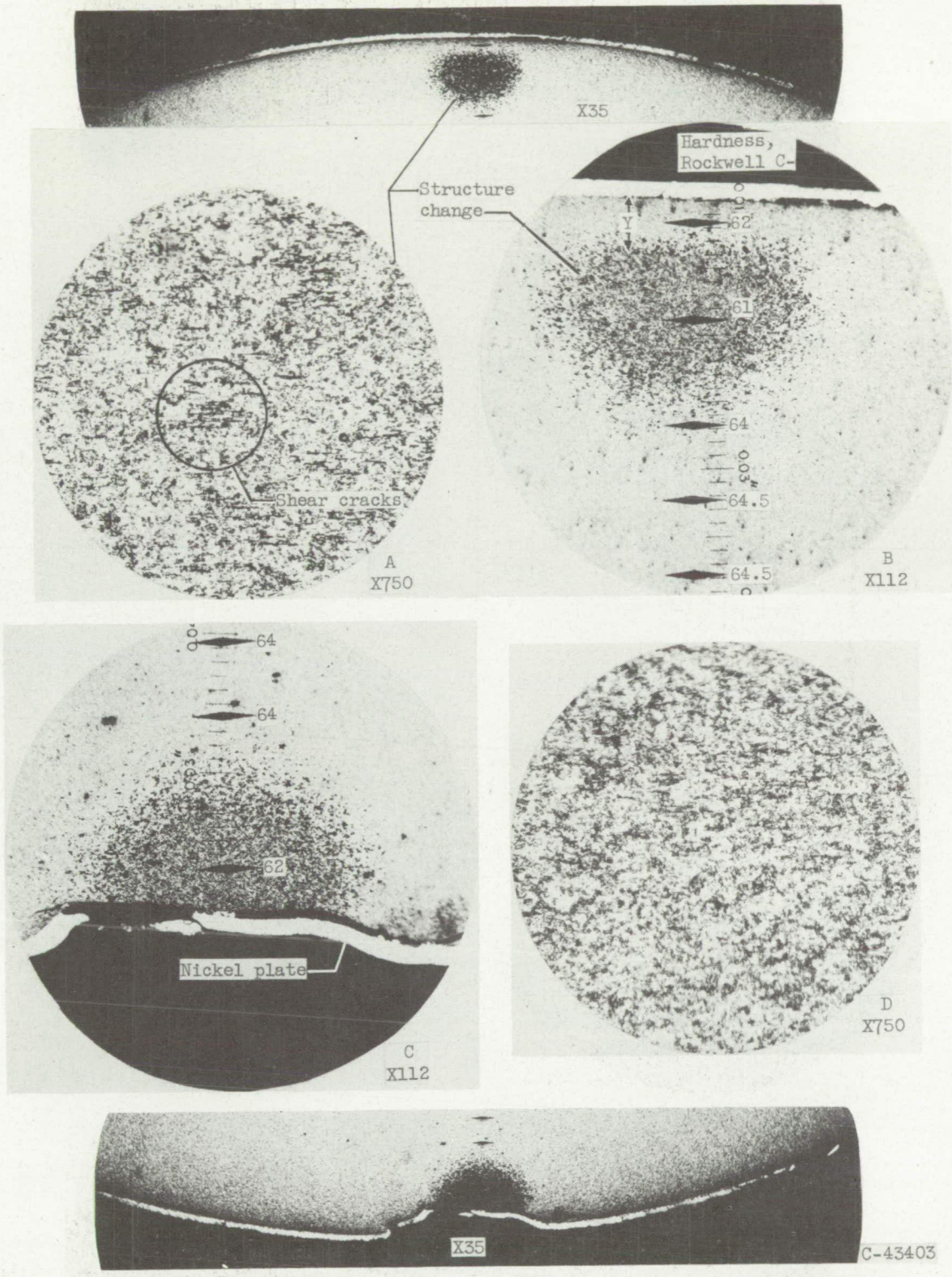

Figure 7. - Structure change in SAE 52100 tested 10×10^7 cycles at 250° F. Transverse views. Figure has been decreased 20 percent in printing.

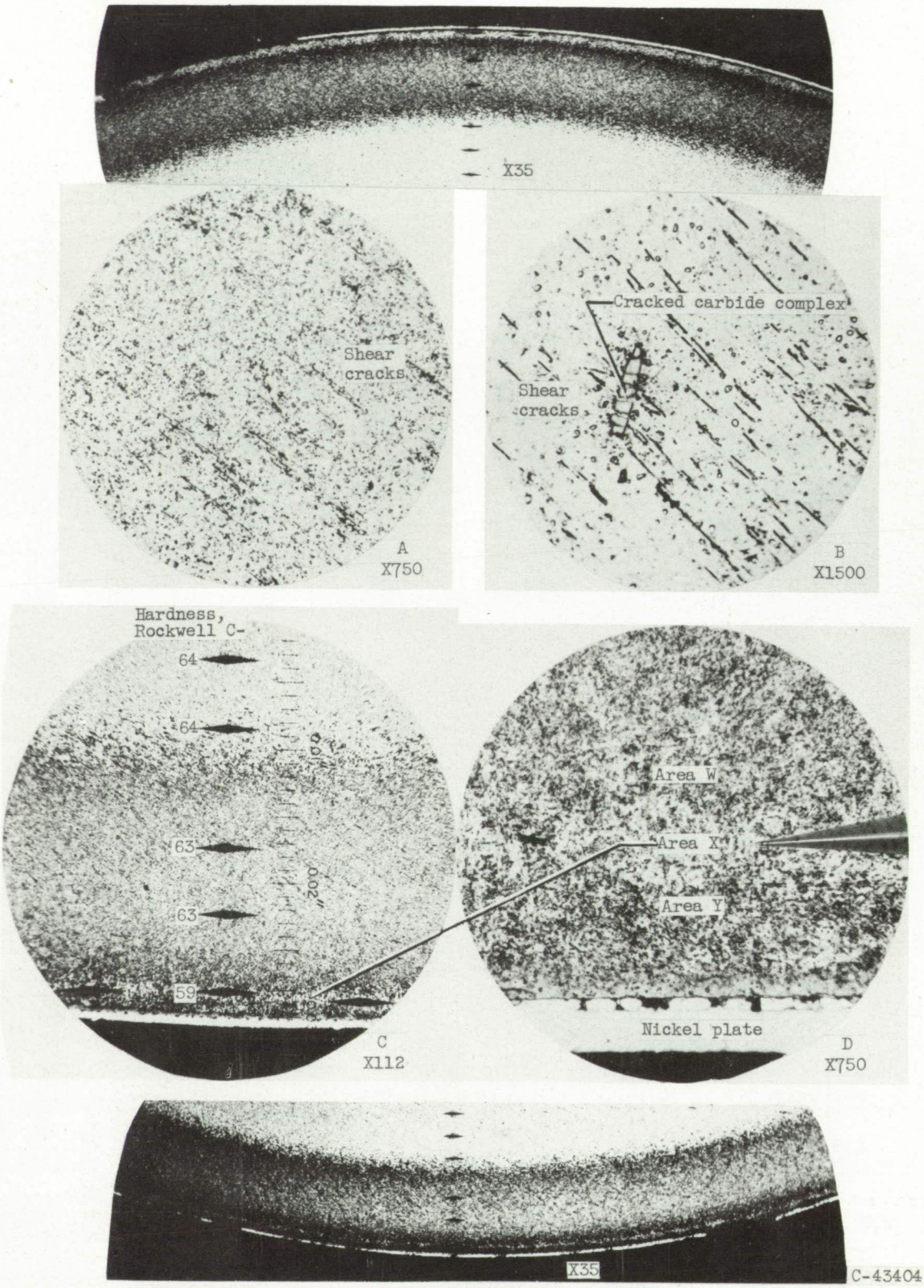

Figure 8. - Structure change in SAE 52100 tested 31×10^7 cycles at 250° F. Longitudinal views. Figure has been decreased 20 percent in printing.

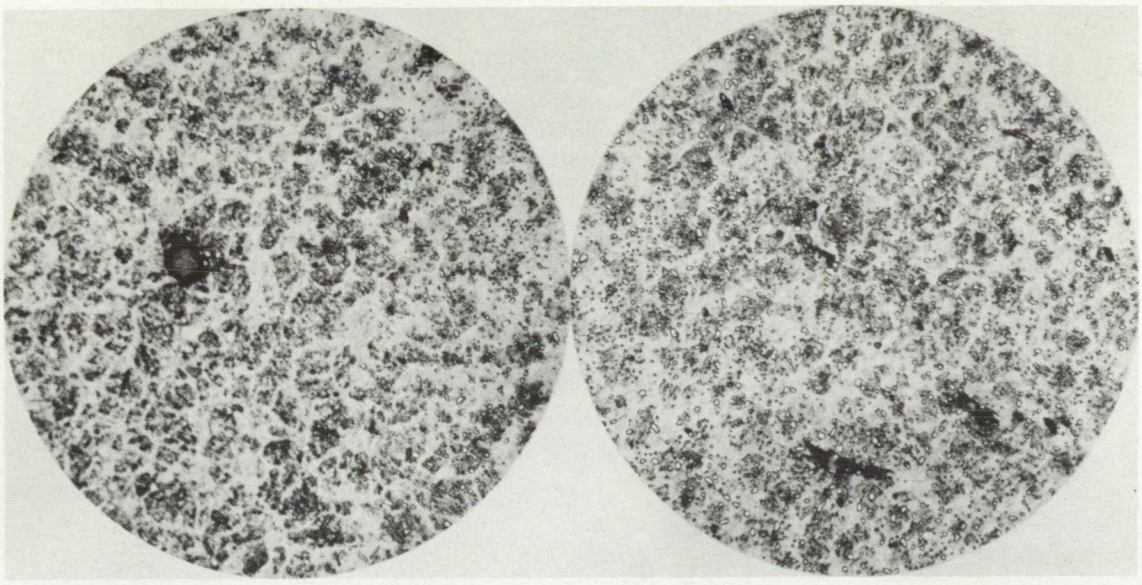

(a) SAE 52100 as received. (b) SAE 52100 after 200×10^7 cycles.

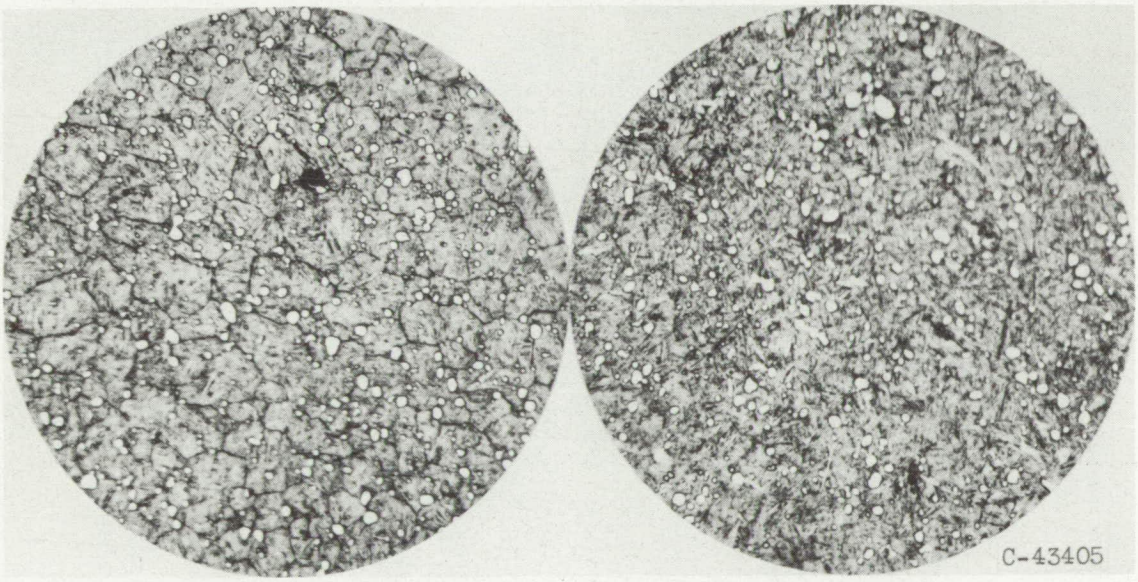

(c) AISI M-1 as received. (d) AISI M-1 after 44×10^7 cycles.

Figure 9. - Typical microstructures before and after testing at room temperature X750. Figure has been decreased 8 percent in printing.

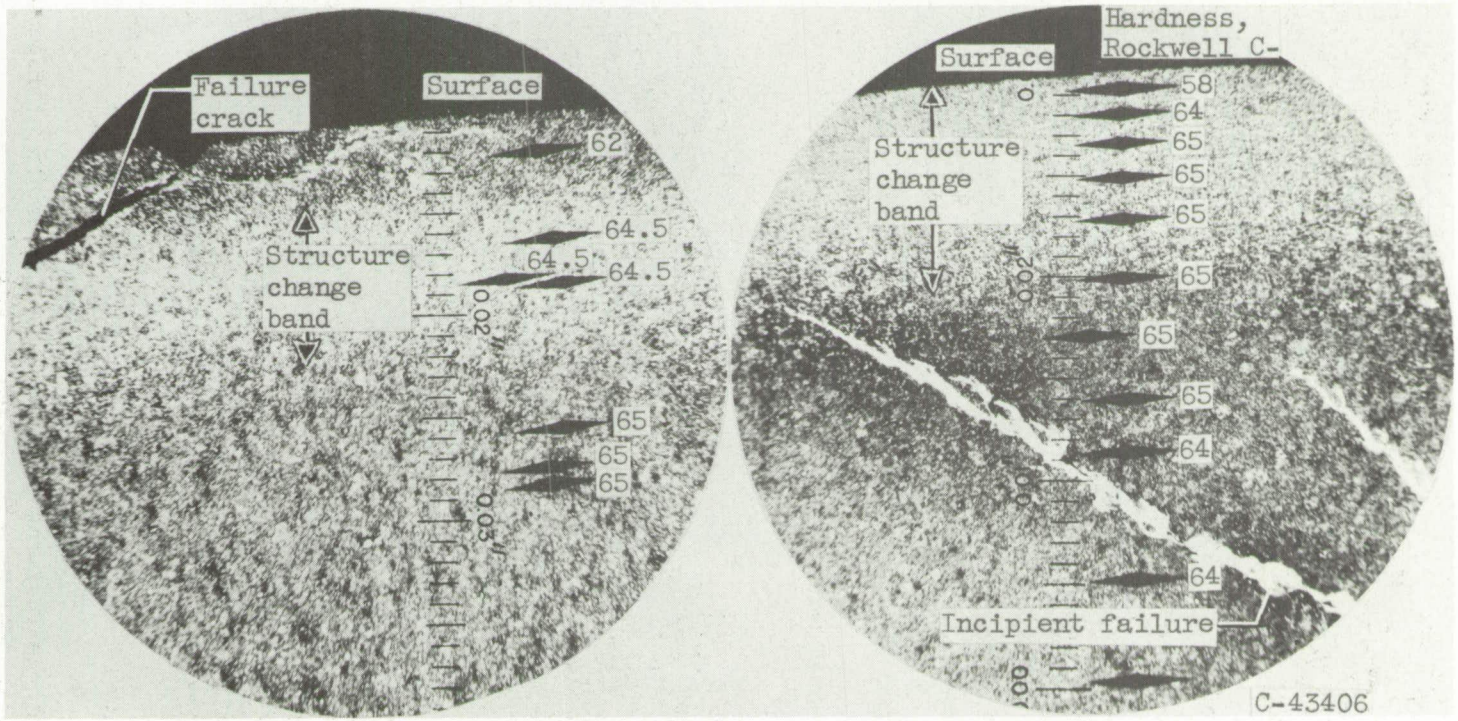

(a) After 15×10^7 cycles.

(b) After 111×10^7 cycles.

Figure 10. - Structure changes in AISI M-1 tested at 200° F. Longitudinal views. X110. Figure has been printed at the original magnification.

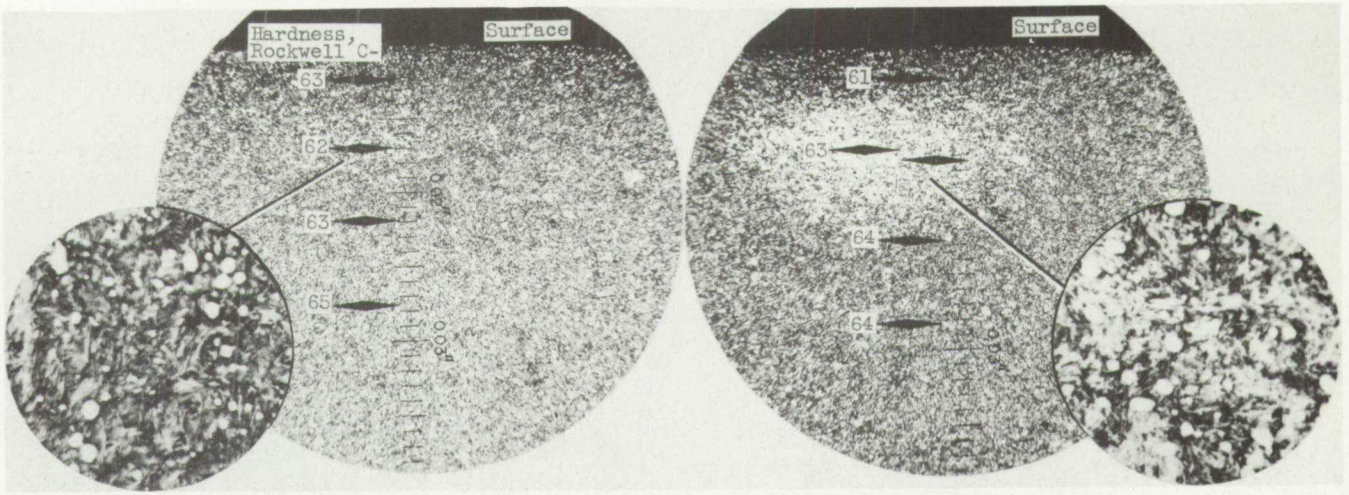

(a) After 4×10^7 cycles.

(b) After 20×10^7 cycles.

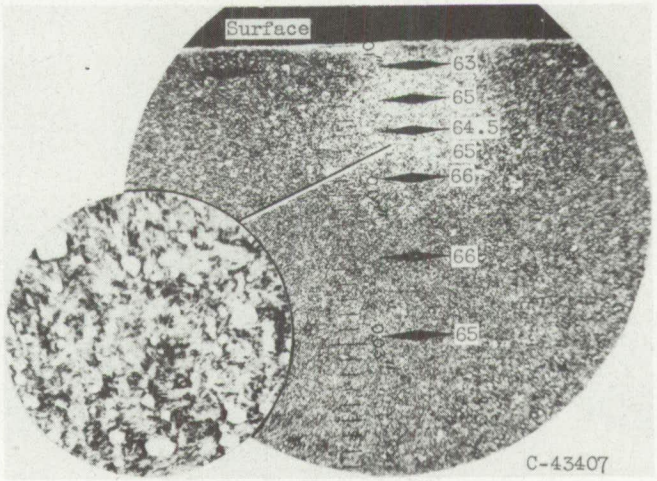

(c) After 111×10^7 cycles.

Figure 11. - Structure changes in AISI M-1 after various testing times. Test temperature, 200° F; transverse views. X110 and X1500. Figure has been decreased 25 percent in printing.

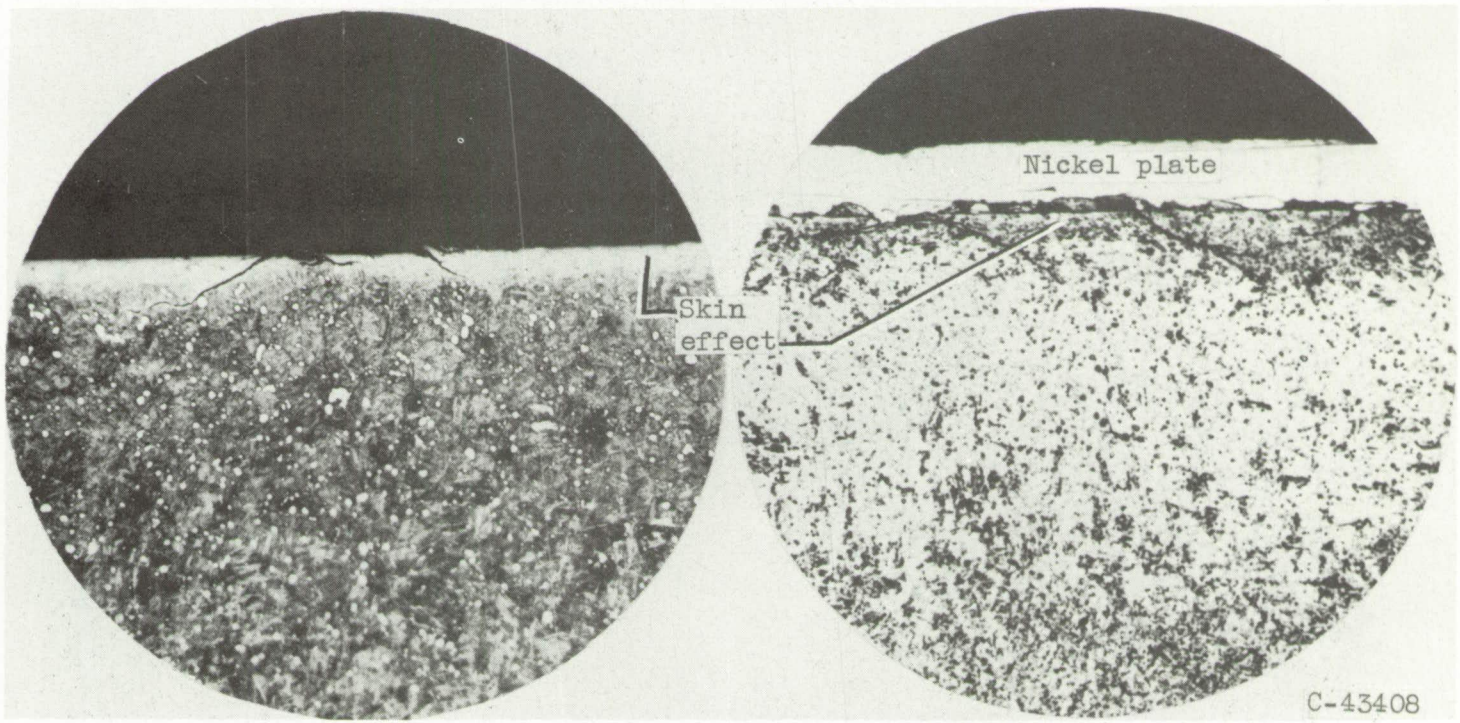

(a) AISI M-1. X500.

(b) SAE 52100. X750.

Figure 12. - Cross section showing ball skin effect. Figure has been printed at original magnification.

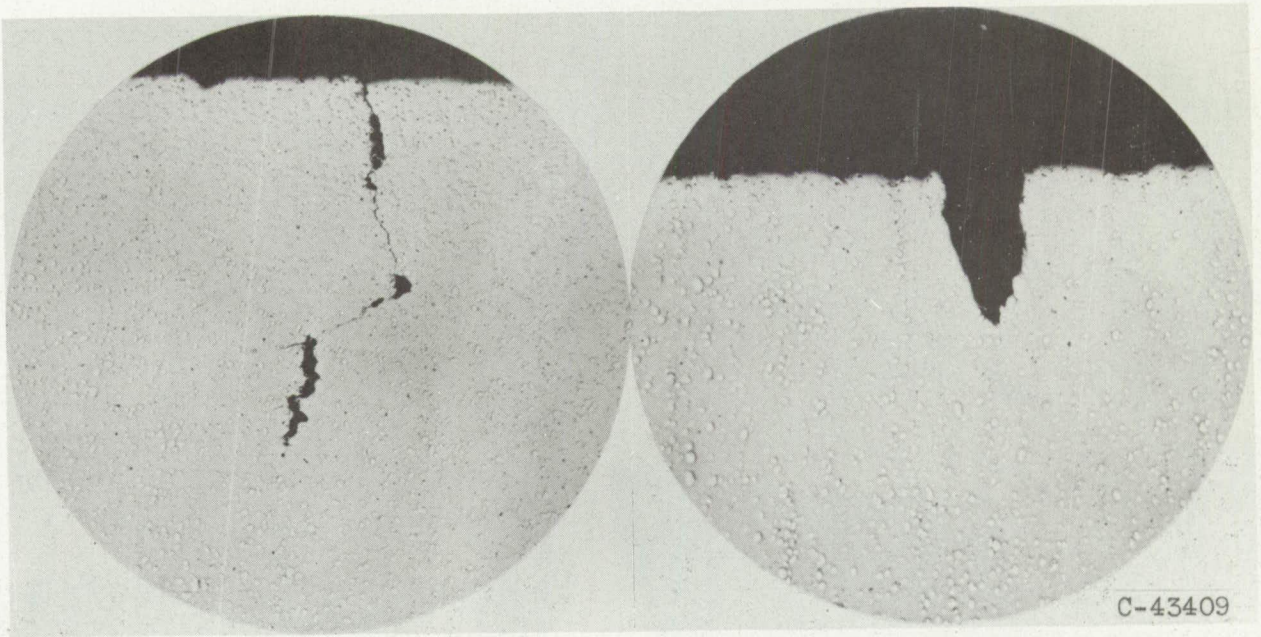

(a) Crack. (b) Large inclusion at surface.

Figure 13. - Defects on as-received AISI M-1 balls. Unetched. X250. Figure has been printed at the original magnification.

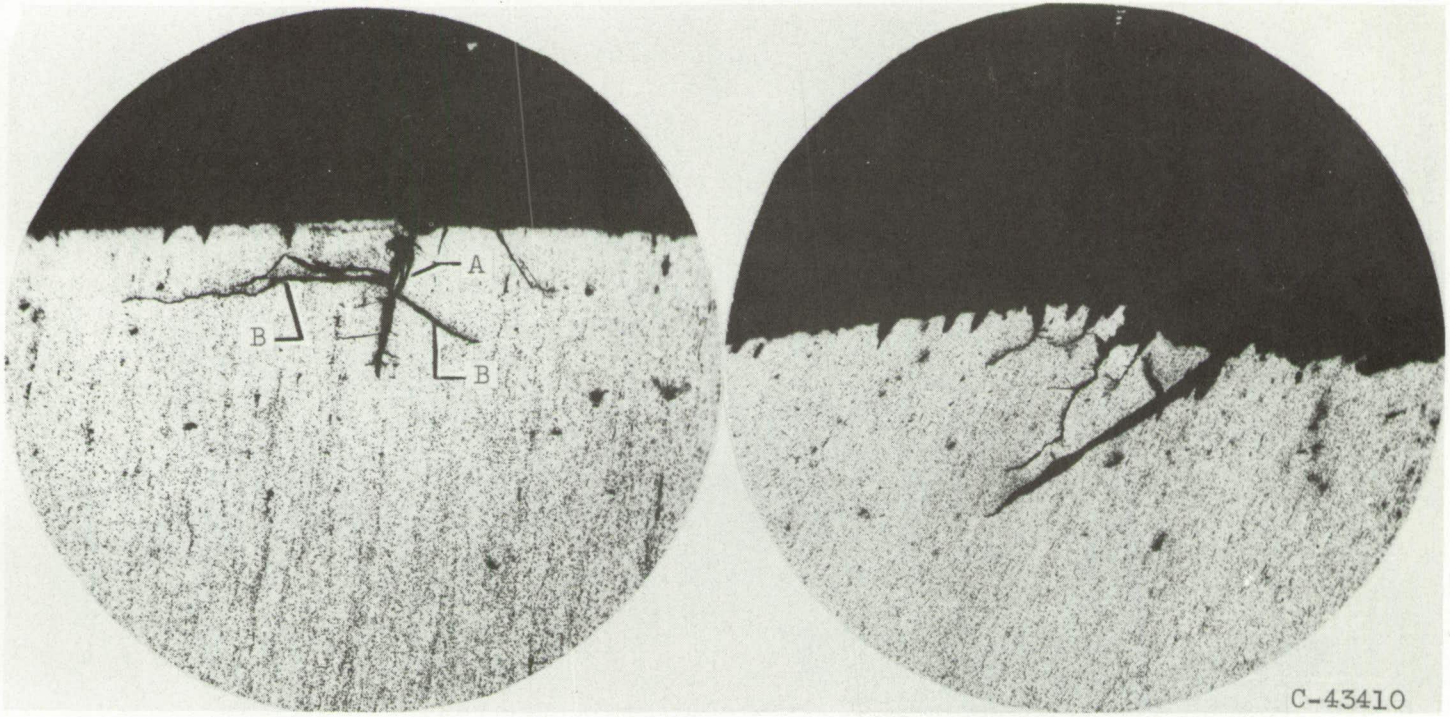

(a) Early stage of failure. X100.

(b) Completed failure. X50.

Figure 14. - SAE 52100 fatigue failure. Room-temperature tests. Figure has been printed at original magnification.

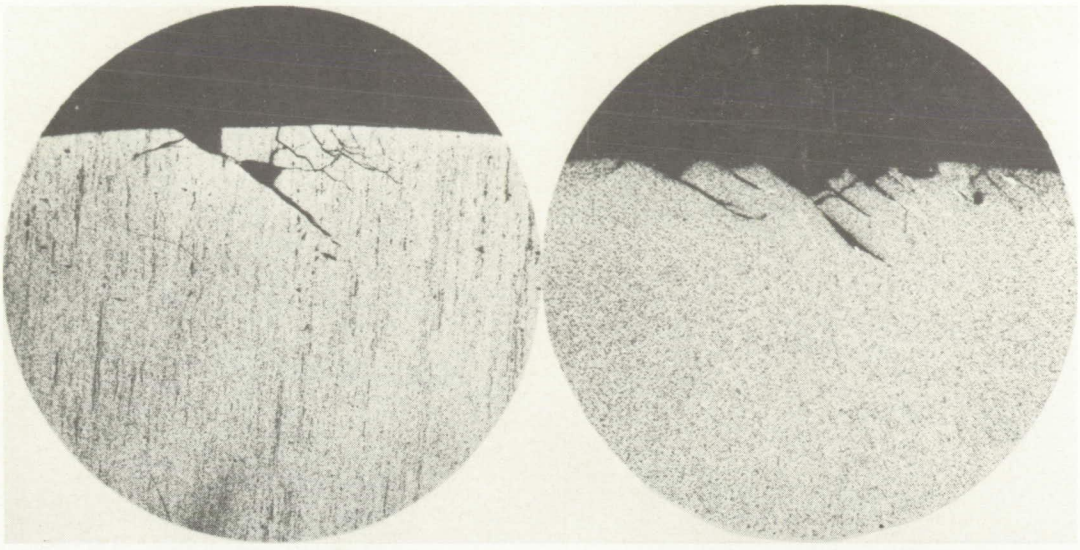

(a) SAE 52100 tested at room temperature. X50.

(b) AISI M-1 tested at room temperature. X50.

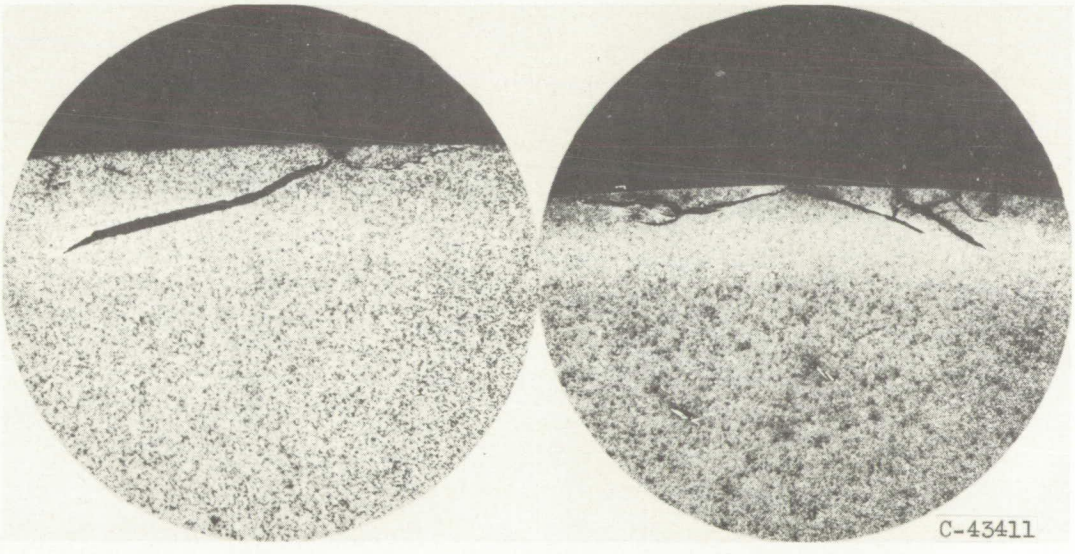

(c) AISI M-1 tested at 200° F. X75.

(d) AISI M-1 tested at 200° F. X50.

Figure 15. - Incompleted fatigue failures showing origin and progression in shear. Figure has been decreased 14 percent in printing.

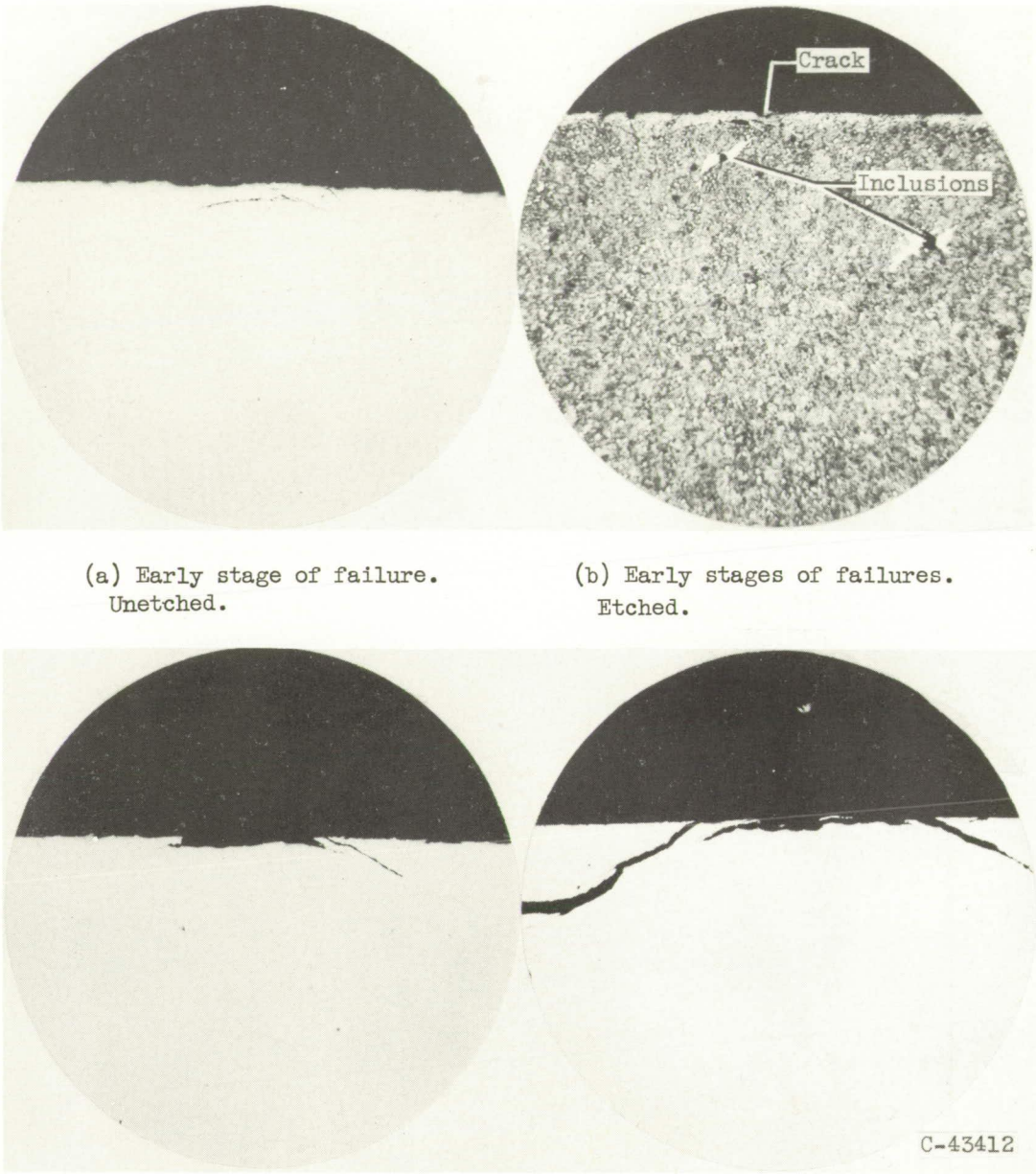

(a) Early stage of failure. Unetched.

(b) Early stages of failures. Etched.

(c) Late stage of failure. Unetched.

(d) Complete failure. Unetched.

Figure 16. - Origin and progression of fatigue failures caused by skin effects and track pitting in AISI M-1. X250. Figure has been decreased 14 percent in printing.